Three-dimensional magnetic resonance imaging of physeal injury: reliability and clinical utility

Lurie, Brett ; Koff, Matthew F ; Shah, Parina ; Feldman, Eric ; Amacker, Nadja ; Downey-Zayas, Timothy ; Green, Daniel ; Potter, Hollis G

Abstract: BACKGROUND: Injuries to the physis are common in children with a subset resulting in an osseous bar and potential growth disturbance. Magnetic resonance imaging allows for detailed assessment of the physis with the ability to generate 3-dimensional physeal models from volumetric data. The purpose of this study was to assess the interrater reliability of physeal bar area measurements generated using a validated semiautomated segmentation technique and to highlight the clinical utility of quantitative 3-dimensional (3D) physeal mapping in pediatric orthopaedic practice. METHODS: The Radiology Information System/Picture Archiving Communication System (PACS) at our institution was searched to find consecutive patients who were imaged for the purpose of assessing a physeal bar or growth disturbance between December 2006 and October 2011. Physeal segmentation was retrospectively performed by 2 independent operators using semiautomated software to generate physeal maps and bar area measurements from 3-dimensional spoiled gradient recalled echo sequences. Inter-reliability was statistically analyzed. Subsequent surgical management for each patient was recorded from the patient notes and surgical records. RESULTS: We analyzed 24 patients (12M/12F) with a mean age of 11.4 years (range, 5-year to 15-year olds) and 25 physeal bars. Of the physeal bars: 9 (36%) were located in the distal tibia; 8 (32%) in the proximal tibia; 5 (20%) in the distal femur; 1 (4%) in the proximal femur; 1 (4%) in the proximal humerus; and 1 (4%) in the distal radius. The independent operator measurements of physeal bar area were highly correlated with a Pearson correlation coefficient (r) of 0.96 and an intraclass correlation coefficient for average measures of 0.99 (95% confidence interval, 0.97-0.99). Four patients underwent resection of the identified physeal bars, 9 patients were treated with epiphysiodesis, and 1 patient underwent bilateral tibial osteotomies. CONCLUSIONS: Semiautomated segmentation of the physis is a reproducible technique for generating physeal maps and accurately measuring physeal bars, providing quantitative and anatomic information that may inform surgical management and prognosis in patients with physeal injury.

DOI: https://doi.org/10.1097/BPO.0000000000000104

DOI: https://doi.org/10.1097/BPO.0000000000000104

Three-dimensional Magnetic Resonance Imaging of Physeal Injury: Reliability and Clinical Utility

Brett Lurie, MBBS, Matthew F. Koff, PhD,* Parina Shah, MS,* Eric James Feldmann, MD,* Nadja Amacker, MD,* Timothy Downey-Zayas, BA,† Daniel Green, MD,† and Hollis G. Potter, MD**

Background: Injuries to the physis are common in children with a subset resulting in an osseous bar and potential growth disturbance. Magnetic resonance imaging allows for detailed assessment of the physis with the ability to generate 3-dimensional physeal models from volumetric data. The purpose of this study was to assess the interrater reliability of physeal bar area measurements generated using a validated semiautomated segmentation technique and to highlight the clinical utility of quantitative 3-dimensional (3D) physeal mapping in pediatric orthopaedic practice.

Methods: The Radiology Information System/Picture Archiving Communication System (PACS) at our institution was searched to find consecutive patients who were imaged for the purpose of assessing a physeal bar or growth disturbance between December 2006 and October 2011. Physeal segmentation was retrospectively performed by 2 independent operators using semiautomated software to generate physeal maps and bar area measurements from 3-dimensional spoiled gradient recalled echo sequences. Inter-reliability was statistically analyzed. Subsequent surgical management for each patient was recorded from the patient notes and surgical records.

Results: We analyzed 24 patients (12M/12F) with a mean age of 11.4 years (range, 5-year to 15-year olds) and 25 physeal bars. Of the physeal bars: 9 (36%) were located in the distal tibia; 8 (32%) in the proximal tibia; 5 (20%) in the distal femur; 1 (4%) in the proximal femur; 1 (4%) in the proximal humerus; and 1 (4%) in the distal radius. The independent operator measurements of physeal bar area were highly correlated with a Pearson correlation coefficient (r) of 0.96 and an intraclass correlation coefficient for average measures of 0.99 (95% confidence interval, 0.97-0.99). Four patients underwent resection of the identified physeal bars, 9 patients were treated with epiphysiodesis, and 1 patient underwent bilateral tibial osteotomies.

Conclusions: Semiautomated segmentation of the physis is a reproducible technique for generating physeal maps and accurately measuring physeal bars, providing quantitative and anatomic information that may inform surgical management and prognosis in patients with physeal injury.

Level of Evidence: Level IV.

Key Words: physis, MRI, segmentation, physeal bar, magnetic resonance imaging

(*J Pediatr Orthop* 2014;34:239–245)

Injuries to the growth plate are common in children and can result in growth disturbance leading to leg-length discrepancy or angular deformity.[1] Fracture is the most frequent cause of injury to the growth plate; however, physeal damage can occur as a result of a variety of processes including infection and tumors.[2] Up to 30% of fractures involve the growth plate,[3] a small subset of which may progress to the formation of an osseous bar leading to potential growth disturbance.

Several systems have been developed to classify fractures and predict the likelihood of growth disturbance.[2–4] Some of these incorporate more complex patterns of fracture and take into account injuries to critical areas of the physis such as the groove of Ranvier and the perichondrial ring of LaCroix, which may be associated with a higher risk of complication.[5,6] In general, Salter-Harris (SH) III, IV, and V fractures have a higher rate of growth disturbance than SH I and II fractures.[7] However, the likelihood of growth arrest is more dependent on the actual path of the fracture through the physis than on the fracture classification.[1]

Surgical management options for the treatment of physeal bars include physeal bar resection, surgical epiphysiodeses, limb lengthening procedures, and corrective osteotomies.[8] The clinical decision-making process is multifactorial, including patient age, remaining growth potential, the location of injury within the physis, and the size of the physeal bar.[9]

We believe that magnetic resonance imaging (MRI) has become the method of choice[10] for imaging physeal injuries because of its superior soft tissue contrast, high resolution, multiplanar capabilities, and lack of ionizing radiation.[11] Three-dimensional (3D), frequency-selective, fat-suppressed gradient recalled echo (3D-SPGR) sequences

From the Departments of *Radiology and Imaging—MRI; and †Orthopedics, Hospital for Special Surgery, New York, NY.

None of the authors received financial support for this study.

H.S.S. has an institutional research agreement in place with General Electric Healthcare. The other authors have no conflict of interest to declare.

Reprints: Hollis G. Potter, MD, Department of Radiology and Imaging—MRI, Hospital for Special Surgery, 535 East 70th Street, West Basement—MRI, New York, NY 10021. E-mail: potterh@hss.edu.

highlight the uninjured open physis as a high signal intensity structure that is clearly distinguishable from the adjacent metaphysis and epiphysis (Fig. 1).[12,13]

Techniques for manually segmenting the physis from volumetric data sets are well described[10,13,14] but can be time consuming. The use of customized semiautomated software for the measurement of physeal bars was recently validated in an animal model demonstrating an excellent correlation between MRI and histologic measurement of physeal bar area.[15] In their study, Koff and colleagues created physeal bars in skeletally immature rabbits with the use of radiofrequency ablation and then demonstrated the accuracy of 3D mapping against histologic measurement of physeal bar area from en bloc surgical resections.

The purpose of this study was to assess the interrater reliability of physeal bar area measurements generated using this semiautomated mapping method when applied clinically and to, therefore, highlight the utility of 3D physeal maps in clinical practice.

METHODS

Patients

Our Institutional Review Board approved the study. We retrospectively searched the Radiology Information System (RIS)/Picture Archiving Communication System (PACS) (Sectra Imtec AB, Linkoping, Sweden) to find consecutive patients who had undergone MRI for physeal bar assessment or growth disturbance between December 2006 and October 2011. Patient's age, sex, anatomic site involved, type of insult, growth disturbance at the time of injury, and clinical outcome were recorded from the RIS/PACS, clinical notes and surgical records as summarized in Table 1.

Imaging

All the patients included in the study have been imaged for clinical reasons, as summarized in Table 1. The 3D-SPGR sequence was routinely acquired for all skeletally immature patients imaged at our institution; these sequences were interpreted qualitatively by the reading radiologist to determine the degree of physeal closure, which was included in the clinical report. Quantitative assessment of the physis was performed upon request by the referring clinician, although 3D maps with area quantitation had been generated for all patients in this study at the time of initial imaging.

Imaging was performed on 1.5 T and 3 T MRI units (GE Healthcare, Waukesha, WI) using dedicated surface coils. The 3D-SPGR was performed in the coronal or sagittal plane depending on the involved physis. The imaging parameters were 3 T/1.5 T, repetition time (10.7/7.1 ms), echo time (1.9/2.4 ms), slice thickness (1.5/1.4 mm), field of view (160 to 120 mm), flip angle (20/10 degrees), matrix ($256 \times 256/256 \times 256$), and pixel bandwidth (325.55/244.14 Hz/pixel).

3D Mapping Technique

Two independent operators with experience in physeal mapping retrospectively analyzed the SPGR

FIGURE 1. A, Coronal intermediate echo time fast spin echo magnetic resonance image demonstrating an osseous bar (black arrow) in an 11-year-old boy following a Salter-Harris IV fracture of the distal femur. B, Coronal fat-suppressed spoiled gradient recalled echo sequences image showing the bar (white arrow) as a low signal intensity transphyseal connection between the metaphysis and epiphysis. The uninjured open physis is hyperintense (white arrowhead).

TABLE 1. Clinical and Imaging Details of Patient Cohort

Case Number	Age (y)	Sex	Body Part	Insult	Leg-length Discrepancy (LLD) or Angular Deformity	Location of Bar	% Bar Reader 1	% Bar Reader 2	Management
1	9	F	Proximal tibia	Blount disease	38 degrees tibia vara, 5 cm LLD	Peripheral	10.8	17.5	Osteotomy
2	5	M	Distal femur	Compound SH IV	2.2 cm LLD	Peripheral	51.8	43.3	Bar resection
3	13	M	Distal tibia	SH II	0.6 cm LLD	Central	28.5	30.9	Epiphysiodesis
4	15	M	Proximal tibia	SH I	None	Peripheral	1.6	1.1	Clinical follow-up
5	13	M	Proximal tibia	SH IV	None	Central	5.5	5.9	Clinical follow-up
6	9	M	Proximal tibia	Blount disease	36 degrees tibia vara	Peripheral	18.4	15.5	Multiple epiphysiodeses
7	9	M	Proximal tibia	Blount disease	18 degrees tibia vara	Peripheral	2.7	1.9	Multiple epiphysiodeses
8	11	M	Distal tibia	SH II	None	Central	28.4	35.8	Bar resection
9	13	F	Proximal tibia	Prior patella re-alignment surgery	None	Central	1.5	1.2	Clinical follow-up
10	9	M	Proximal tibia	SH IV	None	Central	69.5	75.4	Epiphysiodesis
11	11	F	Distal tibia	SH IV	20 degrees varus at the ankle, 1 cm LLD	Linear	12.5	9.9	Epiphysiodesis
12	9	F	Distal tibia	SH IV	None	Linear	38.2	38	Bar resection
13	12	M	Proximal femur	Internal fixation of femoral neck fracture	None	Mixed	38.5	27.3	Clinical follow-up
14	13	F	Distal tibia	SH IV	5 degrees genu varum, 1 cm LLD	Peripheral	21.9	22.8	Clinical follow-up
15	11	F	Distal radius	SH II	None	Central	1.7	1.4	Clinical follow-up
16	11	M	Distal femur	SH II	0.3 cm LLD, bilateral genu varus L > R	Peripheral	10.4	8.1	Multiple epiphysiodeses
17	13	M	Distal femur	SH IV	4 degrees varus LLD 0.4 cm	Central	19.8	16.5	Hemi-epiphysiodesis
18	11	F	Proximal humerus	Pathological fracture through UBC	43 degrees humerus varus, 7.6 cm LLD	Mixed	49	43.6	Epiphysiodesis
19	9	F	Distal tibia	SH II	2.4 cm LLD	Peripheral	16.7	19.3	Epiphysiodesis
20	15	F	Distal femur	SH II	None	Central	16.7	10.9	Clinical follow-up
21	11	M	Distal tibia	SH II	16 degrees tibia vara	Peripheral	3.7	4.4	Clinical follow-up
22	12	M	Distal tibia	Prior distal tibial osteotomy	None	Central	29.5	29.2	Clinical follow-up
23	10	F	Distal femur	Unknown, no trauma/surgery	18 degrees distal femoral valgus	Peripheral	5.7	4.3	Clinical follow-up
24	8	F	Distal tibia	SH II	None	Central	4.7	4.5	Progress MRI at 3 months and then bar resection
25	13	F	Proximal tibia	Osteomyelitis	None	Central	0.9	5.7	Clinical follow-up

MRI indicates magnetic resonance imaging; SH, Salter-Harris.

sequences acquired at the time of the initial MRI examination. The analysis was performed using semi-automated customized software (GE Healthcare) that had been previously validated in a juvenile rabbit model of radiofrequency-ablated physes, using histology as a standard (Fig. 2).[15]

The operator initially set a voxel intensity threshold to only include voxels with signal intensity similar to that of the open physis, which was seen as uniform high signal intensity. The injured physis was intermediate signal intensity, which has been attributed to the presence of hemorrhage, fibrous tissue, or damaged disordered chondrocytes within the physis.[16,17] A mature osseous bar was visualized as low signal intensity blending indistinguishably with the fatty marrow of the adjacent metaphysis and epiphysis (Fig. 3). For the purposes of this study, only mature osseous bars were measured.

Once the intensity threshold had been set, the user then manually selected a voxel within the physis to allow the computer to identify connected physeal voxels and segment the physis across all slices in the series, with the user then manually refining the segmentation as needed. The physeal map was generated utilizing a validated image analysis algorithm[15] to create a 3D model of the uninjured physis. The physeal bar was displayed as a gap in the model, the boundaries of which were defined by the operator. The software then automatically calculated the area of the physeal bar expressed in mm^2 and as a percentage of the whole physis. The physeal bar was classified as peripheral, linear, or central[18] based on its 3D

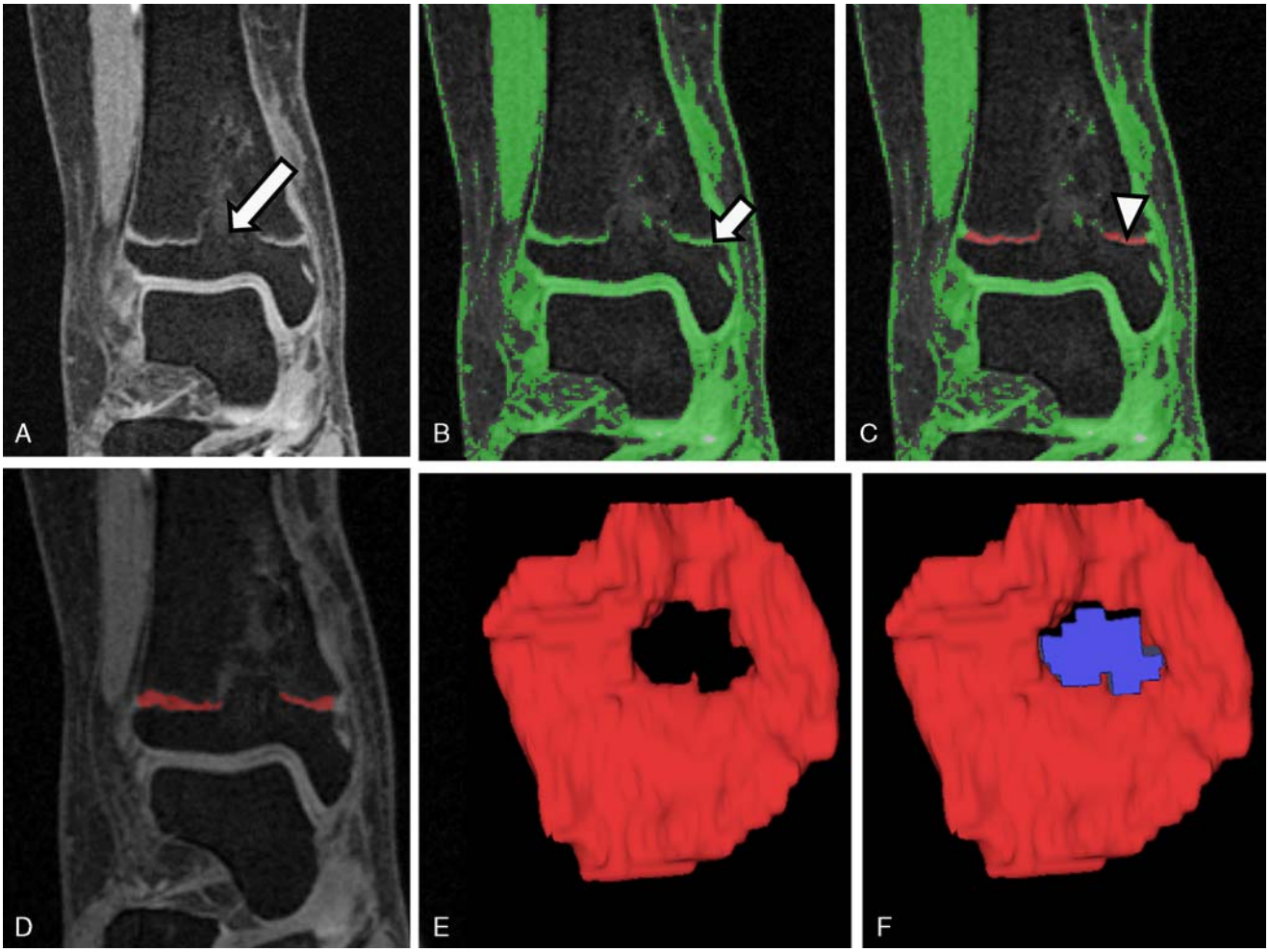

FIGURE 2. Semiautomated segmentation of the physis from a coronal fat-saturated 3-dimensional spoiled gradient recalled echo sequences. A, Unprocessed image demonstrating a mature physeal bar (long white arrow). B, User-defined voxel intensity threshold to include the physis (short white arrow) and voxels of similar intensity. C, User selects a voxel within the physis to allow the software to isolate the physis based on the connectedness of similar intensity voxels across all the slices in the series (arrowhead). D, The refined segmented physis with the threshold removed. E, Three-dimensional map of the uninjured physis with the bar displayed as a gap. F, The filled-in physeal bar in blue allowing automated quantitation.

appearance (Fig. 3). If the bar extended to the periphery of the physis it was classified as peripheral. Narrow bars extending to the anterior and posterior margins of the physis in a sagittal or oblique sagittal plane with intact physis on either side were classified as linear. Bars that were completely surrounded by uninjured physis were classified as central. Those bars that could not be classified as peripheral, linear, or central were recorded as mixed. As the software used in this study was highly customized for physeal assessment, very minimal operator training (< 1 h) was required to utilize the software. Both operators were able to generate the 3D map and bar measurements in < 10 minutes per patient.

Analysis

The 2 independently obtained physeal bar area measurements were compared with assess interrater reliability between the 2 operators. Statistical analysis was performed using a Pearson correlation coefficient (r). Deviations of measurements were reported as systematic (comparison of pairwise differences including +/− offsets) and absolute deviations (comparison of pairwise differences not including +/− offset). Interrater agreement was also assessed using an intraclass correlation coefficient. Statistical analysis was performed with SPSS, Version 20.0. (IBM Corp., Armonk, NY).

RESULTS

Our initial search yielded 26 patients. After patients without physeal bars were excluded (n = 2), a total of 24 patients and 25 physeal bars were analyzed. Fifty percent of patients were male individuals (n = 12) and 50% were female individuals (n = 12), ranging in age from 5 to 15 years with a mean age of 11.4 years. Of the physeal bars, 36% (n = 9) were located in the distal tibia, 32% (n = 8)

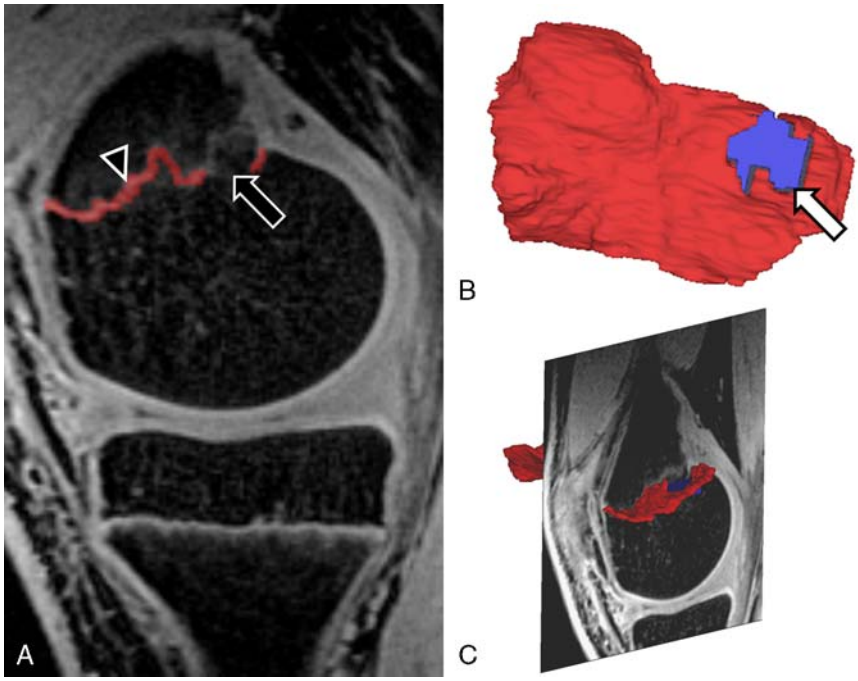

FIGURE 3. Three-dimensional physeal segmentation in a 15-year-old adolescent with growth arrest following a Salter-Harris II fracture of the distal femur. A Initial segmentation (black arrowhead) of the 3-dimensional spoiled gradient recalled echo sequences sagittal magnetic resonance imaging showing a physeal bar (black arrow). B, Three-dimensional physeal map demonstrating the peripheral location, small size, and rounded shape of the physeal bar relative to the uninjured physis (white arrow). C, Physeal map superimposed on the source image.

proximal tibia, 20% (n = 5) distal femur, 4% (n = 1) proximal femur, 4% (n = 1) proximal humerus, and 4% (n = 1) distal radius. The most common insult was fracture observed in 64% (n = 16) of patients. Two patients had Blount disease, which was bilateral in one case and analyzed separately (cases 6 and 7). Three patients had physeal injuries related to prior surgeries. One patient sustained a pathologic fracture through a unicameral bone cyst of the proximal humerus, 1 patient had osteomyelitis, and in 1 case the initial insult was unknown. The demographics, initial insults, and involved physes of our patients were concordant with the literature.[3,6,10,12,13,19]

The mean size of mature osseous bars ranged from 2.3% to 73% of the physis as summarized in Table 1. Of the 25 physeal bars, 44% (n = 11) were classified as central, 40% (n = 10) peripheral, 8% (n = 2) linear, and 8% (n = 2) mixed. Both linear bars formed as a result of a Salter-Harris IV fracture.

The independent measurements of physeal bar area by operators 1 and 2 were highly correlated with a Pearson correlation coefficient (r) of 0.96 and an intraclass correlation coefficient for average measures of 0.99 (95% confidence interval, 0.97-0.99).

The largest relative discrepancy in operator measurements was case 25. The cause of this discrepancy was the presence of tiny immature physeal bridges adjacent to the main area of mature osseous bridging, which had fallen just below the user-specified voxel intensity threshold set by operator 1 but was included by operator 2.

Those patients who underwent bar resection tended to be slightly younger ranging from ages 5 to 9 years old. The resected bars constituted < 50% of the physis. Of the resected bars: 2 were central; 1 peripheral; and 1 linear.

The 2 patients with Blount disease (case 1 and cases 6 and 7) underwent angular corrective surgery and multiple surgical epiphysiodeses of the distal femoral and proximal tibial epiphyses to prevent leg-length discrepancy and correct existing angular deformities. In the 7 patients who underwent epiphysiodesis, the decision to operate was based on individual patient factors including age, bone age, and existing leg-length discrepancies. Patients 13, 14, 20, and 22 with higher percentage physeal bars underwent shorter term clinical follow-up that included follow-up MRI. In case 24, initial imaging following physeal insult demonstrated an osseous bar only involving 4.6% of the physis; however, the remainder of the physis demonstrated altered signal intensity suggestive of more extensive physeal injury, for which short-term follow-up was suggested. Three months later, a repeat MRI demonstrated a 20% mature osseous bar that was then resected.

DISCUSSION

The surgical decision-making process for managing physeal injuries is complex and patient specific,[9] highlighting the need for the accurate anatomic information provided by 3D-MRI. MRI is the method of choice for

evaluation of the physis and physeal injuries.[10] Physeal sensitive volumetric pulse sequences like 3D-SPGR with frequency-selective fat suppression permit postacquisition generation of 3D physeal maps to display the physis and to accurately measure the area of physeal damage, which in our experience is extremely useful in shaping surgical management and for discussions with patients and their families.

Quantitation of physeal bars can be achieved without semiautomated software by creating a maximum intensity projection (MIP) image from an axial MRI series, which is achievable on most modern PACS systems.[12] Quantitation off MIP images is more difficult as the boundaries of the physeal bar are less clearly defined. The MIP images also do not demonstrate the undulations of the physis and cannot be manipulated in 3 dimensions. Manual segmentation of the physis can also be achieved using standard commercially available software as described by Craig et al[10] using a "paint-on-slice" approach, although these techniques are relatively time consuming, require a high degree of manual dexterity, and are subject to greater interrater variability.

The semiautomated quantitative technique we have described is advantageous because it is faster than manual segmentation of the physis and is therefore potentially more applicable to routine assessment of physeal injuries. As we have shown, semiautomated measurement of the physis is also highly reproducible as the 3D maps and quantitative measurements are based on voxel intensity thresholds. High-contrast, high-definition, 3D models can also be manipulated in 3 dimensions for surgical approach planning.

In our experience, the location, size, and geometry of the physeal bar is much more easily appreciated on 3D maps than on stacked 2-dimensional images, which aids in the surgical decision-making process. Accurate knowledge of the location of a bar within the physis is vital as peripheral bars may be amenable to direct visualization from the periphery of the physis, whereas central bridge resection may require a more difficult surgical approach from above or below the physis to avoid unnecessary damage to the healthy physis.[8]

Animal models suggest that osseous bars involving $>7\%$ of the growth plate are likely to result in growth arrest, whereas those $<7\%$ may break spontaneously with growth of the uninjured physis.[20] It is also known that bridge excisions with interposition of an inert material, such as fat, have a higher success rate when $<50\%$ and ideally, $<25\%$ of the physis is involved.[12] It is therefore clear that accurate quantitative assessment of physeal bar area provides important prognostic information and informs appropriate surgical management in the setting of physeal bar formation.

Although it is clear that sufficiently large osseous bars lead to growth disturbance,[20] the prognostic significance of areas of nonosseous physeal signal abnormality is currently unknown and warrants further study. With the advent of semiautomated physeal segmentation techniques, it may be possible to quickly provide maps of osseous bridging, as well as maps of physeal signal

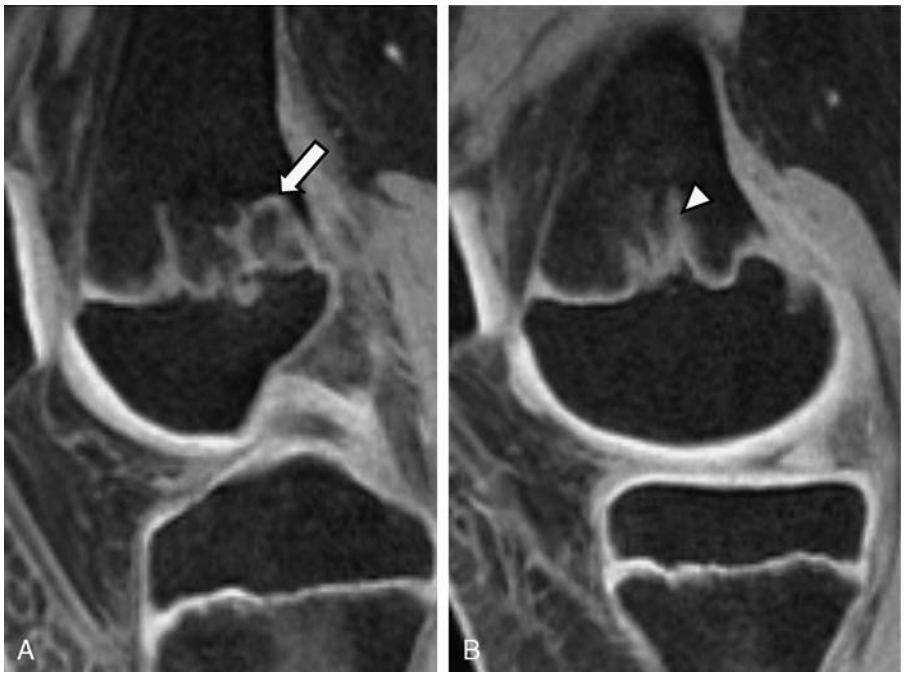

FIGURE 4. Sagittal fat-suppressed 3-dimensional spoiled gradient recalled echo sequences magnetic resonance images in a 13-year-old adolescent with a prior Salter-Harris IV fracture of the distal femur demonstrating metaphyseal intrusions as (A) bars of cartilage signal intensity within the metaphysis (arrow); (B) direct extensions of cartilage from the physis (arrowhead).

abnormality that potentially reflect physeal dysfunction. Although many physeal injuries heal spontaneously without the formation of an osseous bar,[1] large areas of physeal dysfunction could indicate the need for short-term follow-up imaging to detect early osseous bridging (as observed in case 24 of our series). Although prophylactic physeal surgery before the formation of an osseous bar is not common,[21] the need for early recognition of osseous physeal bridging to prevent the complications of growth disturbance and avoid corrective surgeries is well established.[22]

Pathologic osseous bar formation is indistinguishable from areas of physiological physeal closure, which is particularly problematic as patients approach skeletal maturity. Knowledge of the patterns of physiological closure of different physes and their expected appearance as maturity approaches is vital to contextual interpretation of physeal maps. Patient factors, the nature of injury, and the appearance of adjacent physes in the imaging field of view are all useful in aiding interpretation. We have demonstrated the high interrater reliability of semiautomated 3D physeal mapping across a wide range of growth plates, in patients at different stages of skeletal maturity with assorted growth plate insults.

Previous investigators[1,10,23] have reported several associated imaging findings in the setting of physeal injury, which we observed in our patients. Metaphyseal intrusions can be seen as projections emanating from the physis or as islands of cartilage adjacent to the growth plate (Fig. 4). These metaphyseal irregularities are evidence of previous physeal insult or transient loss of physeal blood supply and have been attributed to disturbances in chondrocyte maturation and degeneration.[1] A similar pathophysiological mechanism may account for growth plate widening.[7]

The current study has some limitations derived from its retrospective design and associated bias in patient selection. Because of the geometric limitations of tissue received at the time of surgery, which are not en bloc resections, we could not histologically confirm our physeal bar area measurements in those patients who underwent bar resection, although the software used was previously validated with careful MRI-histologic correlation in a rabbit model.[15] We also acknowledge that the particular semiautomated software used in this study is not currently commercially available, although we have endeavored to discuss some alternative approaches to physeal segmentation for those wishing to apply this technique to their own clinical practice.

We have demonstrated that semiautomated segmentation of the physis is a reproducible technique for the generation of 3D physeal maps in a cohort of patients with varied physeal insults affecting a range of different growth plates, at different stages of skeletal maturity. Quantitative assessment of physeal injuries and 3D physeal maps are important for surgical decision making and can be generated in a fast and reproducible manner using a semiautomated technique.

REFERENCES

1. Ecklund K, Jaramillo D. Imaging of growth disturbance in children. *Radiol Clin North Am*. 2001;39:823–841.
2. Ogden JA. *Skeletal Injury in the Child*. New York: Springer; 2000.
3. Peterson HA, Madhok R, Benson JT, et al. Physeal fractures: Part 1. Epidemiology in Olmsted County, Minnesota, 1979-1988. *J Pediatr Orthop*. 1994;14:423–430.
4. Salter RB, Harris WR. Injuries involving the epiphyseal plate. *J Bone Joint Surg*. 1963;45:587–622.
5. Oestreich AE, Ahmad BS. The periphysis and its effect on the metaphysis: I. Definition and normal radiographic pattern. *Skeletal Radiol*. 1992;21:283–286.
6. Dodwell ER, Kelley SP. Physeal fractures: basic science, assessment and acute management. *Orthop Trauma*. 2011;25:377–391.
7. Ogden JA. Injury to the growth mechanisms of the immature skeleton. *Skeletal Radiol*. 1981;6:237–253.
8. Marsh JS, Polzhofer GK. Arthroscopically assisted central physeal bar resection. *J Pediatr Orthop*. 2006;26:255–259.
9. Kelley BGESP, Kelley SP. Management of traumatic physeal growth arrest. *Orthop Trauma*. 2012;26:200–211.
10. Craig JGJ, Cramer KEK, Cody DDD, et al. Premature partial closure and other deformities of the growth plate: MR imaging and three-dimensional modeling. *Radiology*. 1999;210:835–843.
11. Potter HG, Schachar J. High resolution noncontrast MRI of the hip. *J Magn Reson Imaging*. 2010;31:268–278.
12. Ecklund K, Jaramillo D. Patterns of premature physeal arrest: MR imaging of 111 children. *AJR Am J Roentgenol*. 2002;178:967–972.
13. Sailhan FDR, Chotel F, Guibal A-L, et al. Three-dimensional MR imaging in the assessment of physeal growth arrest. *Eur Radiol*. 2004;14:1600–1608.
14. Borsa JJ, Peterson HA, Ehman RL. MR imaging of physeal bars. *Radiology*. 1996;199:683–687.
15. Koff MF, Chong LR, Virtue P, et al. Correlation of magnetic resonance imaging and histologic examination of physeal bars in a rabbit model. *J Pediatr Orthop*. 2010;30:928–935.
16. Synder M, Harcke HT, Bowen JR, et al. Evaluation of physeal behavior in response to epiphysiodesis with the use of serial magnetic resonance imaging. *J Bone Joint Surg Am*. 1994;76:224–229.
17. Khoshhal KI, Kiefer GN. Physeal bridge resection. *J Am Acad Orthop Surg*. 2005;13:47–58.
18. Peterson HAH. Partial growth plate arrest and its treatment. *J Pediatr Orthop*. 1984;4:246–258.
19. Craig JG, Cody DD, van Holsbeeck M. The distal femoral and proximal tibial growth plates: MR imaging, three-dimensional modeling and estimation of area and volume. *Skeletal Radiol*. 2004;33:337–344.
20. Guzzanti V, Falciglia F, Gigante A, et al. The effect of intra-articular ACL reconstruction on the growth plates of rabbits. *J Bone Joint Surg Br*. 1994;76:960–963.
21. Foster BK, John B, Hasler C. Free fat interpositional graft in acute physeal injuries: the anticipatory Langenskiold procedure. *J Pediatr Orthop*. 2000;20:282–285.
22. Loraas EK, Schmale GA. Endoscopically aided physeal bar takedown and guided growth for the treatment of angular limb deformity. *J Pediatr Orthop B*. 2011;21:348–351.
23. Laor T, Jaramillo D. MR imaging insights into skeletal maturation: what is normal? *Radiology*. 2008;250:28–38.